

# Suppression of narrow-band transparency in a metasurface induced by a strongly enhanced electric field

Yasuhiro Tamayama,<sup>1,\*</sup> Keisuke Hamada,<sup>1</sup> and Kanji Yasui<sup>1</sup>

<sup>1</sup>*Department of Electrical, Electronics and Information Engineering,  
Nagaoka University of Technology, 1603-1 Kamitomioka, Nagaoka, Niigata 940-2188, Japan*

(Dated: October 12, 2015)

We realize a suppression of an electromagnetically induced transparency (EIT) like transmission in a metasurface induced by a local electric field that is strongly enhanced based on two approaches: squeezing of electromagnetic energy in resonant metasurfaces and enhancement of electromagnetic energy density associated with a low group velocity. The EIT-like metasurface consists of a pair of radiatively coupled cut-wire resonators, and it can effect both field enhancement approaches simultaneously. The strongly enhanced local electric field generates an air discharge plasma at either of the gaps of the cut-wire resonators, which causes the EIT-like metasurface to change into two kinds of Lorentz type metasurfaces.

PACS numbers: 78.67.Pt, 41.20.Jb, 78.20.Ci, 42.65.Pc

## I. INTRODUCTION

There has been considerable interest in controlling electromagnetic waves using metamaterials. Metamaterials are artificial continuous media made of arrays of subwavelength structures. The electromagnetic response of a metamaterial is determined by the shape, material, and distribution of its unit structure, and therefore metamaterials with desired characteristics can be realized by designing the structure of the unit cell.

One of the most promising applications of metamaterials is the realization of highly nonlinear media [1]. In a metamaterial composed of resonant structures such as split-ring resonators, electromagnetic energy is squeezed into small volume regions of the metamaterial [2]. Nonlinear elements located in these regions exhibit enhanced nonlinear responses owing to the compression of the electromagnetic field. To date, enhancement of harmonic generations [3–10], bistable media [11–13], tunable media [4, 11, 14, 15], and modulation instability [16] have been experimentally investigated using resonant metamaterials.

Another strategy for enhancing nonlinear phenomena is to decrease the energy velocity, which is equal to the group velocity of electromagnetic waves in lossless media [17]. The electromagnetic energy density increases with decreasing energy velocity [18] and therefore the interaction between the electromagnetic wave and the nonlinear medium is enhanced.

If the above two approaches for enhancing nonlinear phenomena are integrated, nonlinear phenomena can be further enhanced. Although the effects of the two approaches are not clearly separable in resonant metamaterials, the resonant enhancement of nonlinearity can be maximized by using the group velocity as a index of the field enhancement. In this study, as a verification of this concept, we realize a change of an electromagnetic response of a metasurface induced by a strongly enhanced

electromagnetic field. A metasurface that mimics electromagnetically induced transparency (EIT) [19–30] is used to simultaneously realize squeezing of the electromagnetic energy and a low group velocity. The response of the EIT-like metasurface is theoretically analyzed based on an electrical circuit model of its unit structure to show the condition for minimizing the group velocity, i.e., maximizing the electric field enhancement factor. The maximum enhancement factor is examined through measurement and numerical analysis of the linear characteristics of the metasurface. The strongly enhanced electric field generates an air discharge plasma in the metasurface, which causes a change in its effective structure.

## II. THEORY

The characteristics of the EIT-like metasurface used in this study are theoretically analyzed based on the electrical circuit model of its unit structure shown in Fig. 1(a) to clarify the method for decreasing the group velocity, i.e., enhancing the local electric field. The electrical circuit consists of two inductor-capacitor series resonant circuits coupled via a mutual impedance  $Z_M = R_M - i[\omega M - (\omega C_M)^{-1}]$ , where  $\omega$  is the angular frequency of the voltage sources that correspond to the incident wave. The following assumptions are made in the analysis below to simplify the calculation. (1) The circuit constants satisfy  $L_1 = L_2 = L_0$ ,  $C_1 \simeq C_2$ ,  $R_1 = R_2 = R_0$ ,  $V_1 = V_2$ , and  $\text{Im}(Z_M) = 0$ . The first four conditions imply that the characteristics of the two resonators are the same except for the resonant frequency and that the resonant frequencies are close to each other. The last equation implies that the resonators are coupled only via indirect coupling, i.e., radiative coupling [31, 32]. (2) The electric dipole moment of the unit cell of the metasurface is proportional to the sum of the stored charges in the two capacitors. Applying Kirch-

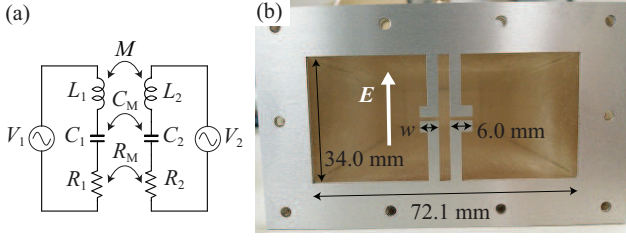


FIG. 1. (a) Electrical circuit model for the unit cell of the EIT-like metasurface. (b) Photograph of the fabricated metasurface.

hoff's voltage law to the electrical circuit and using the above assumptions, the electric susceptibility  $\chi_e$  of the metasurface at around  $\omega \simeq \omega_0$  can be written as follows:

$$\chi_e \approx \frac{-\alpha(\omega^2 - \omega_0^2 + i\gamma_L\omega)}{(\omega^2 - \omega_0^2 + i\gamma_0\omega)^2 - [(\omega_2^2 - \omega_1^2)/2]^2 + (\omega R_M/L_0)^2}, \quad (1)$$

where  $\omega_{1,2} = 1/\sqrt{L_0 C_{1,2}}$ ,  $\omega_0^2 = (\omega_1^2 + \omega_2^2)/2$ ,  $\gamma_0 = R_0/L_0$ ,  $\gamma_L = \gamma_0 - (R_M/L_0)$ , and  $\alpha$  is a proportionality constant. The right-hand side of Eq. (1) is similar to the electric susceptibility of EIT [30]. The EIT-like transparency occurs at an incident angular frequency of  $\omega_0 \approx (\omega_1 + \omega_2)/2$ . Note that  $\gamma_L$  represents the dissipated power from the resonators that does not contribute to the indirect coupling, because  $\gamma_0$  represents the total power dissipated from each resonator and  $R_M/L_0$  represents the radiative coupling between the resonators. Assuming that the group index at  $\omega = \omega_0$  is much larger than the refractive index, the group index at  $\omega = \omega_0$  is then written as follows:

$$n_g \approx \frac{\alpha(\Delta^2 - \gamma_L^2)}{(\Delta^2 + 2\gamma_0\gamma_L - \gamma_L^2)^2}, \quad (2)$$

where  $\Delta = |\omega_1 - \omega_2|$ . When  $\gamma_L \ll \gamma_0$ , the right-hand side of Eq. (2) exhibits a maximum value of  $\alpha/8\gamma_0\gamma_L$  at  $\Delta = \sqrt{2\gamma_0\gamma_L} = \Delta_{\max}$ . It can be confirmed from a simple calculation that the stored charge in each capacitor at the transparency frequency also exhibits a maximum at  $\Delta = \Delta_{\max}$ . This implies that the local electric field in the metasurface becomes largest when the group index is maximized.

It is found from the above analysis that a reduction of  $\gamma_L$  is essential for increasing the maximum group index and the electric field enhancement factor. In order to decrease  $\gamma_L$ , nonradiative losses such as dielectric loss and Ohmic loss should be suppressed and the radiation modes of the two resonators should be similar to each other.

We designed and fabricated the EIT-like metasurface shown in Fig. 1(b) based on the above considerations. The structure was cut from an aluminum plate with a thickness of 1.0 mm using wire electrical discharge machining. The unit cell of the metasurface consists of two

kinds of cut-wire resonators. The resonator at the right-hand side is referred to as resonator L and the left-hand side resonator is referred to as resonator H. (In this experiment, the dimension  $w$  in resonator H, indicated in Fig. 1(b), is smaller than 6.0 mm, the length of the corresponding dimension in resonator L, and the resonant frequency of resonator L is therefore lower than that of resonator H.) The two cut-wire resonators are arranged so that the radiation from one resonator can excite the other resonator, that is, the two resonators are indirectly coupled. Since the resonators resemble each other in shape, their radiation modes are similar. The metasurface is made only of aluminum, which behaves as a perfect electric conductor in the microwave region, and thus no dielectric or Ohmic loss occur in the metasurface. Therefore, a small  $\gamma_L$  can be achieved in this metasurface.

### III. LINEAR CHARACTERISTICS OF THE METASURFACE

First, we measured the linear transmission characteristics of the fabricated metasurfaces with various  $w$  to confirm the above theory and to find the condition that realizes the maximum group index, i.e., the maximum local electric field enhancement. The metasurface was placed in a rectangular waveguide and the transmission and group delay spectra of the metasurface were measured using a network analyzer. A thru-reflection-load (TRL) calibration [33] was used to eliminate errors caused by multiple reflections and transmission losses in the experimental system.

Figure 2(a) shows the measured transmission spectrum of the metasurface with  $w = 5.7$  mm. An EIT-like transmission window with a center frequency of 3.036 GHz and a bandwidth of 4 MHz is observed. The difference between the transmission dip frequencies, which are almost the same as the resonant frequencies of the two cut-wire resonators [30], is 42.5 MHz. This value is much smaller than the resonance linewidth of the cut-wire resonators,  $\gamma_0/2\pi = 920$  MHz, which was determined from the decay rate of the stored energy in the cut-wire resonator calculated using a finite-difference time-domain method (not shown). Thus,  $\gamma_L$  is confirmed to be much smaller than  $\gamma_0$ .

Figure 2(b) shows the measured group delay at the transparency frequency for five different metasurfaces with  $w = 5.0$  mm, 5.5 mm, 5.6 mm, 5.7 mm, and 5.8 mm as solid circles in order from right to left. Here  $\Delta/2\pi$  is approximated by the difference between the two transmission dip frequencies. The measured group delay reaches a maximum value of 91 ns at  $w = 5.7$  mm. Assuming that the effective thickness of the metasurface is equal to the thickness of the aluminum plate, the maximum group delay corresponds to a group index of  $2.7 \times 10^4$ . A theoretical fit of the measured data to

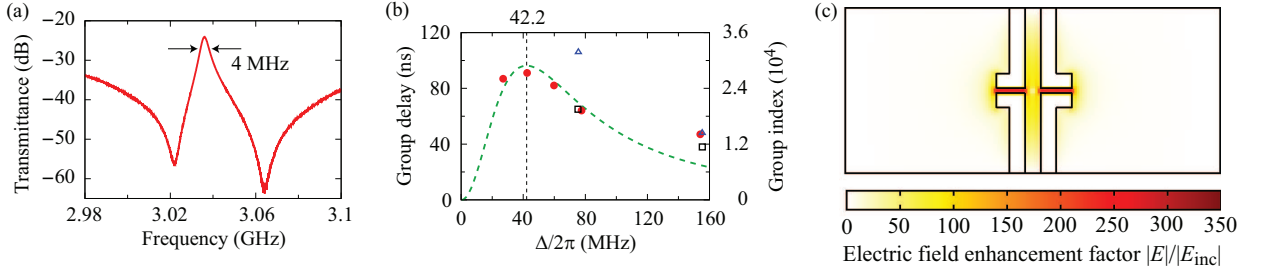


FIG. 2. (a) Linear transmission spectrum for  $w = 5.7$  mm. (b) Measured group delay at the transparency frequency for  $w = 5.0$  mm, 5.5 mm, 5.6 mm, 5.7 mm, and 5.8 mm in order from right to left (solid circles) and theoretical fit according to Eq. (2) (dashed curve). The open squares and triangles represent the numerically analyzed values for  $\sigma = 5.0 \times 10^4$  S/m and  $1.0 \times 10^5$  S/m, respectively. (c) Distribution of numerically calculated ratio of the electric field amplitude  $|E|$  to the incident electric field amplitude  $|E_{\text{inc}}|$  for  $w = 5.7$  mm and  $\sigma = 5.0 \times 10^4$  S/m.

Eq. (2) is shown by the dashed curve. The measured values and fitted curve are in good agreement except for the case of  $w = 5.0$  mm. This difference may be due to the assumptions used in deriving Eq. (2) and by the fact that  $\gamma_L$  varies among the fabricated samples (as described below). The fitted curve exhibits a maximum at  $\Delta/2\pi = 42.2$  MHz, which is almost equal to  $\Delta/2\pi$  for the case of  $w = 5.7$  mm. Therefore, the metasurface with  $w = 5.7$  mm is confirmed to have the optimum condition for maximizing the group index and the electric field enhancement factor at the transparency frequency.

The electric field distribution in the metasurface was analyzed using a finite-difference time-domain method to estimate the electric field enhancement factor. The effective conductivity  $\sigma$  of the aluminum in this experiment needs to be evaluated for the calculation of the enhancement factor. The calculated group delays at the transparency frequency for  $\sigma = 5.0 \times 10^4$  S/m and  $1.0 \times 10^5$  S/m are shown as the open squares and open triangles, respectively, in Fig. 2(b). (The calculations were performed only for the cases of  $w = 5.0$  mm and 5.5 mm due to the limitations of memory and computing time.) The measured values seem to be in the range of the calculated values for  $\sigma = 5.0 \times 10^4$  S/m and  $1.0 \times 10^5$  S/m. Thus, the effective conductivity of the aluminum in this experiment is of the order of  $5 \times 10^4$  S/m to  $1 \times 10^5$  S/m. Figure 2(c) shows the numerically calculated electric field enhancement factor for  $w = 5.5$  mm and  $\sigma = 5.0 \times 10^4$  S/m. The maximum enhancement factor of about 300 is observed at the gaps of the cut-wire resonators. The enhancement factor for  $w = 5.7$  mm would be larger than this value because the group delay for  $w = 5.7$  mm is larger than that for  $w = 5.5$  mm.

Here we discuss the meaning of the effective conductivity in the above simulation. The effective conductivity represents the leak of the indirect coupling as well as the Ohmic loss. If the surface roughness of the cut edge of the metasurface is not much smaller than the skin depth of the metal, the surface current flow is affected by the

surface roughness. As a result, mismatch between the radiation modes of the two cut-wire resonators increases and the leak of the indirect coupling increases. That is,  $\gamma_L$  in Eqs. (1) and (2) increases. It is difficult to directly deal with the surface roughness of the metal in the simulation, while both of the leak of the indirect coupling and the Ohmic loss are the factors that increase  $\gamma_L$ . Therefore, the leak caused by the surface roughness is treated as a factor that decreases the conductivity in the simulation. Since the surface roughness may vary among the fabricated samples, the effective conductivity varies among the samples. In fact, we have already confirmed that  $\gamma_L$  varies between the samples with the same geometrical parameters that were fabricated using different methods. The effective conductivity in this experiment is much smaller than the conductivity of bulk aluminum,  $3.8 \times 10^7$  S/m. This implies that the leak of the indirect coupling caused by the surface roughness is much larger than the Ohmic loss.

#### IV. NONLINEAR CHARACTERISTICS OF THE METASURFACE

Next, we investigated the nonlinear response of the metasurface induced by the strongly enhanced electric field. Hereafter, the metasurface with  $w = 5.7$  mm is used. The experimental setup is shown in Figs. 3(a) and 3(b). A continuous wave generated from a microwave signal generator was amplified and then fed into the rectangular waveguide. The wave was incident onto the metasurface in the waveguide. The transmitted wave was attenuated and then fed into a spectrum analyzer. The rectangular waveguide was placed in a vacuum chamber made of acrylic where the pressure of air was reduced to 1.0 kPa. The TRL calibration was not carried out in this experiment and the total transmittance from the output port of the signal generator to the input port of the spectrum analyzer was measured.

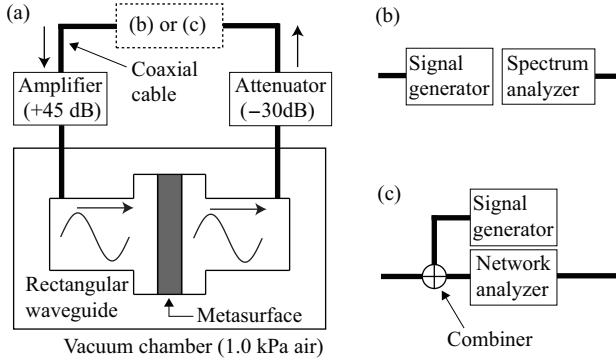


FIG. 3. (a) Experimental setup for the measurement of the nonlinear characteristics of the metasurface. The dashed rectangle represents the setup shown in (b) and (c). (b) Setup for the continuous wave measurement and (c) setup for the pump-probe measurement.

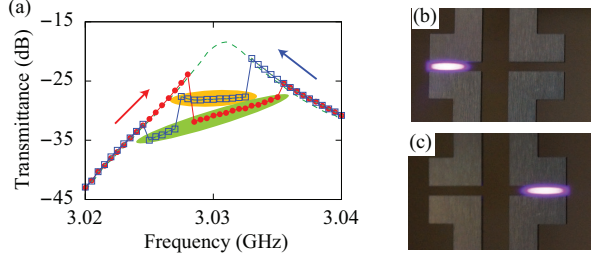


FIG. 4. (a) Transmission spectra of the metasurface with  $w = 5.7$  mm for an incident power of 7.9 W. The red solid circles and blue open squares represent the transmittance when the incident frequency is swept from low to high and from high to low frequencies, respectively. When transmittance in the yellow or green region is observed, the discharge occurs in resonator H or resonator L, respectively. The solid lines are guides for the eye. The green dashed curve represents the linear transmission spectrum. (b) and (c) Photographs of the metasurface when the discharge occurs in resonator H and resonator L, respectively.

Figure 4(a) shows the measured transmission spectra of the metasurface for an incident power of 7.9 W. The red solid circles and blue open squares represent the transmittance when the incident frequency is swept from low to high and from high to low frequencies, respectively. (Harmonic generations were not observed in this experiment.) The green dashed curve represents the linear transmission spectrum that was measured for an incident power below 2.8 W, which corresponds to an incident electric field amplitude of 15 V/cm. There is a frequency region where the transmittance becomes smaller than the linear transmittance at around 3.03 GHz. This observation implies that discharge of air occurs in the metasurface in this frequency region. One of the gaps of the cut-wire resonators is filled by an air plasma, which behaves as a conductor, because of the discharge; thus, the

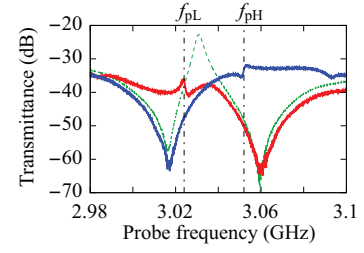


FIG. 5. Transmission spectra of the metasurface with  $w = 5.7$  mm for the probe wave when the discharge is induced in resonator L (red solid curve) and resonator H (blue solid curve) by the pump wave with frequency of  $f_{pL} = 3.024$  GHz and  $f_{pH} = 3.052$  GHz, respectively. The pump power is 15.8 W. The green dashed curve represents the transmission spectrum without the pump wave.

transparency condition collapses and the transmittance decreases. When transmittance in the yellow or green region is observed, the discharge occurs in resonator H or resonator L, respectively. This is because the electric field enhancement is larger in resonator H than in resonator L for a frequency larger than the transmission peak frequency, and vice versa for a frequency smaller than the transmission peak frequency. The discharge starts in the resonator if the local electric field enhancement in the resonator is larger than that in the other resonator and the local electric field exceeds the breakdown electric field. Figures 4(b) and 4(c) show photographs of the metasurface when the discharge occurs in resonator H and resonator L, respectively. Purple light emission due to the discharge is observed. The results of this experiment indicate that the discharge can be induced at either of the gaps by controlling the frequency and power of the incident wave owing to the enhancement of the local electric field.

Finally, the transmission spectrum of the metasurface for a probe wave was measured under irradiation by a pump wave that controls the discharge in the metasurface. The experimental setup is shown in Figs. 3(a) and 3(c). A signal generator was used to generate the pump wave and a network analyzer was used to generate and detect the probe wave. The power of the probe wave was set to be small enough not to affect the discharge state.

Figure 5 shows examples of the measured transmission spectra of the probe wave for a pump power of 15.8 W. The red (blue) solid curve shows the spectrum when the discharge occurs in resonator L (resonator H) and the pump frequency is 3.024 GHz (3.052 GHz). The green dashed curve is the spectrum without the pump wave. Note that the transmittance in this figure represents the total transmittance from the transmitting port to the receiving port of the network analyzer. When a discharge occurs in the metasurface, one of the transmission dips disappears, which causes the transmission peak to dis-

appear. One of the cut-wire resonators changes to resemble a continuous wire, which is a non-resonant structure, because of the air plasma created by the discharge. Only the resonant spectrum of the cut-wire resonator where the discharge does not occur is observed. That is, the EIT-like metasurface is changed into two kinds of Lorentz-type metasurfaces by controlling the frequency and power of the pump wave. In this experiment, simultaneous disappearance of both transmission dips is not observed at any pump frequencies even for a pump power of 15.8 W, which is 5.6 times as large as the threshold incident power for the discharge. This implies that the discharge does not simultaneously occur at both gaps of the cut-wire resonators for an incident power of 15.8 W. It is confirmed from this observation that the electric field enhancement in the metasurface is stronger than that in each constituent resonator, which is caused by the integration of the two approaches for the field enhancement.

The above results show that the metasurface exhibits the EIT-like (Lorentz type) response when the pump wave is turned off (on). The transmission of the probe wave can be controlled by the pump wave like in the original EIT though the dependence of the transmission on the pump wave is opposite to the EIT. So to speak, electromagnetically induced suppression of narrowband transparency is realized in the metasurface. It may be possible to store the probe wave in the metasurface by controlling the pump wave as in the case of the EIT.

Note that all the experiments in this study are highly reproducible. Any deterioration of the characteristics of the metasurface has not been caused by the discharge in our experiment where the incident power is less than 15.8 W (which is the maximum output power of the used amplifier).

## V. CONCLUSION

In conclusion, we have realized the suppression of an EIT-like transmission in the metasurface induced by a strongly enhanced local electric field. To strongly enhance the local electric field, we integrated two approaches: squeezing of electromagnetic energy in resonant metamaterials and enhancement of electromagnetic energy density associated with a low group velocity. The EIT-like metasurface composed of a pair of indirectly coupled cut-wire resonators was used as a metasurface for which the above two approaches can be used simultaneously. The structure of the metasurface was designed and fabricated based on the theoretical analysis of the electrical circuit model of the EIT-like metasurface. An electric field enhancement factor of about 300 was achieved by maximizing the group delay in the metasurface. Owing to the strongly enhanced local electric field, discharge could occur at either of the gaps of the cut-wire resonators. A pump-probe experiment demonstrated that

the EIT-like metasurface was changed into two kinds of Lorentz-type metasurfaces by controlling the power and frequency of the pump wave. The present metasurface can be applied to limiters and switches for electromagnetic waves. It may also be possible to realize memories for electromagnetic waves and to efficiently generate various nonlinear phenomena. In addition, this metasurface could be used for the simple generation of plasma, which can contribute to material processing, chemical reactions, and other applications.

This research was supported by a Grant-in-Aid for Scientific Research on Innovative Areas (No. 22109004) from the Ministry of Education, Culture, Sports, Science, and Technology of Japan, and by a Grant-in-Aid for Research Activity Start-up (No. 25889028) from the Japan Society for the Promotion of Science.

---

\* tamayama@vos.nagaokaut.ac.jp

- [1] M. Lapine, I. V. Shadrivov, and Y. S. Kivshar, *Rev. Mod. Phys.* **86**, 1093 (2014).
- [2] J. B. Pendry, A. J. Holden, D. J. Robbins, and W. J. Stewart, *IEEE Trans. Microwave Theory Tech.* **47**, 2075 (1999).
- [3] M. W. Klein, C. Enkrich, M. Wegener, and S. Linden, *Science* **313**, 502 (2006).
- [4] I. V. Shadrivov, A. B. Kozyrev, D. W. van der Weide, and Y. S. Kivshar, *Appl. Phys. Lett.* **93**, 161903 (2008).
- [5] E. Kim, F. Wang, W. Wu, Z. Yu, and Y. R. Shen, *Phys. Rev. B* **78**, 113102 (2008).
- [6] A. Rose, D. Huang, and D. R. Smith, *Phys. Rev. Lett.* **107**, 063902 (2011).
- [7] T. Kanazawa, Y. Tamayama, T. Nakanishi, and M. Kitano, *Appl. Phys. Lett.* **99**, 024101 (2011).
- [8] T. Nakanishi, Y. Tamayama, and M. Kitano, *Appl. Phys. Lett.* **100**, 044103 (2012).
- [9] R. Czaplicki, H. Husu, R. Siikanen, J. Mäkitalo, M. Kauranen, J. Laukkanen, J. Lehtolahti, and M. Kuittinen, *Phys. Rev. Lett.* **110**, 093902 (2013).
- [10] K. O'Brien, H. Suchowski, J. Rho, A. Salandrino, B. Kante, X. Yin, and X. Zhang, *Nature Mater.* **14**, 379 (2015).
- [11] B. Wang, J. Zhou, T. Koschny, and C. M. Soukoulis, *Opt. Express* **16**, 16058 (2008).
- [12] M. Lapine, I. V. Shadrivov, D. A. Powell, and Y. S. Kivshar, *Nature Mater.* **11**, 30 (2012).
- [13] M. Liu, Y. Sun, D. A. Powell, I. V. Shadrivov, M. Lapine, R. C. McPhedran, and Y. S. Kivshar, *Phys. Rev. B* **87**, 235126 (2013).
- [14] D. A. Powell, I. V. Shadrivov, and Y. S. Kivshar, *Appl. Phys. Lett.* **95**, 084102 (2009).
- [15] E. Poutrina, D. Huang, and D. R. Smith, *New. J. Phys.* **12**, 093010 (2010).
- [16] Y. Tamayama, T. Nakanishi, and M. Kitano, *Phys. Rev. B* **87**, 195123 (2013).
- [17] T. F. Krauss, *Nature Photon.* **2**, 448 (2008).
- [18] P. Y. Chen, R. C. McPhedran, C. M. de Sterke, C. G. Poulton, A. A. Asatryan, L. C. Botten, and M. J. Steel, *Phys. Rev. A* **82**, 053825 (2010).

- [19] V. A. Fedotov, M. Rose, S. L. Prosvirnin, N. Papasimakis, and N. I. Zheludev, Phys. Rev. Lett. **99**, 147401 (2007).
- [20] S. Zhang, D. A. Genov, Y. Wang, M. Liu, and X. Zhang, Phys. Rev. Lett. **101**, 047401 (2008).
- [21] P. Tassin, L. Zhang, T. Koschny, E. N. Economou, and C. M. Soukoulis, Phys. Rev. Lett. **102**, 053901 (2009).
- [22] N. Liu, L. Langguth, T. Weiss, J. Kästel, M. Fleischhauer, T. Pfau, and H. Giessen, Nature Mater. **8**, 758 (2009).
- [23] Y. Tamayama, T. Nakanishi, Y. Wakasa, T. Kanazawa, K. Sugiyama, and M. Kitano, Phys. Rev. B **82**, 165130 (2010).
- [24] L. Zhang, P. Tassin, T. Koschny, C. Kurter, S. M. Anlage, and C. M. Soukoulis, Appl. Phys. Lett. **97**, 241904 (2010).
- [25] C. Kurter, P. Tassin, L. Zhang, T. Koschny, A. P. Zhuravel, A. V. Ustinov, S. M. Anlage, and C. M. Soukoulis, Phys. Rev. Lett. **107**, 043901 (2011).
- [26] Y. Tamayama, T. Nakanishi, and M. Kitano, Phys. Rev. B **85**, 073102 (2012).
- [27] J. Gu, R. Singh, X. Liu, X. Zhang, Y. Ma, S. Zhang, S. A. Maier, Z. Tian, A. K. Azad, H.-T. Chen, A. J. Taylor, J. Han, and W. Zhang, Nature Commun. **3**, 1151 (2012).
- [28] T. Nakanishi, T. Otani, Y. Tamayama, and M. Kitano, Phys. Rev. B **87**, 161110 (2013).
- [29] F. Miyamaru, H. Morita, Y. Nishiyama, T. Nishida, T. Nakanishi, M. Kitano, and M. W. Takeda, Sci. Rep. **4**, 4346 (2014).
- [30] Y. Tamayama, K. Yasui, T. Nakanishi, and M. Kitano, Phys. Rev. B **89**, 075120 (2014).
- [31] S. Zhang, Z. Ye, Y. Wang, Y. Park, G. Bartal, M. Mrejen, X. Yin, and X. Zhang, Phys. Rev. Lett. **109**, 193902 (2012).
- [32] L. Verslegers, Z. Yu, Z. Ruan, P. B. Catrysse, and S. Fan, Phys. Rev. Lett. **108**, 083902 (2012).
- [33] *Agilent Network Analysis Applying the 8510 TRL Calibration for Non-Coaxial Measurements* (2001).